Controllable production of degenerate Fermi gases of 6Li atoms in the crossover from two dimensions to three dimensions

Hongwei Gong,[1] Haotian Liu [●],[1] Bolong Jiao,[1] Haoyi Zhang,[1] Hang Yu [●],[1] Qinxuan Peng,[1] Shuai Peng [●],[1] Tangqian Shu,[1] Yan Zhu,[1] Jiaming Li [●],[1,2,3,*] and Le Luo [●][1,2,3,†]

[1]*School of Physics and Astronomy, Sun Yat-sen University, Zhuhai, Guangdong 519082, China*
[2]*Center of Quantum Information Technology, Shenzhen Research Institute of Sun Yat-sen University, Shenzhen, Guangdong 518087, China*
[3]*State Key Laboratory of Optoelectronic Materials and Technologies, Sun Yat-Sen University, Guangzhou 510275, China*

Many-body physics in dimensional crossover systems has attracted much attention, but is yet to explore intensively. Cold atoms provide an excellent experimental platform to address the questions in this area, but technical difficulties still exist. When an optical lattice is applied to tune the dimensionality of trapped cold atoms, it is usually difficult to precisely tune the occupation ratio of the atom in the different lattice bands. In this paper we report the method to tune the occupation ratio of the energy band when transferring a three-dimensional Fermi gas into a one-dimensional optical lattice, where we could tune the occupation ratio in the lowest band from unity to 50% quantitatively by jointly varying the trapping potentials of the optical dipole trap and the one-dimensional lattice. This method provides a route to study the dependence of the many-body interaction on the dimensionality by continuously changing the dimensionality of a Fermi gas in the crossover from two dimensions to three dimensions.

I. INTRODUCTION

Experiments of two-dimensional (2D) Fermi gases have attracted significant interest since they provide a highly controllable tool to explore many-body physics in the flatland. The experimental progress includes the preparation and production of a 2D Fermi gas [1,2], the observation of a dimension-modified interaction [3] and polaron [4,5], thermodynamic measurements of the equations of the state [6–9], the radio-frequency spectrum [10–14], observation of paring and the Berezinskii-Kosterlitz-Thouless phase transition [15–18], the measurements of transport properties [19–21], the measurements of the collective mode for a quantum anomaly [22–25], and the realization of the Josephson junction [26]. So far, most of these experiments have focused on the dependence of many-body effects on interaction strength and temperature. On the other hand, the relation between many-body effects and the dimensionality crossover is much less explored [2,12,24,27], partially limited by the lack of a capability to continuously tune the occupation ratio of the different lattice bands. With this capability, it is expected that the fascinating physics in this crossover regime could be explored, such as Tan's contact with noninteger dimensionality, the dimensional evolution of a quantum anomaly, and the higher temperature superfluidity.

In this paper we report the production of degenerate Fermi gases of 6Li atoms in the crossover from two dimensions to three dimensions with the tunable occupation ratio of the ground and first excited bands in a 1D optical lattice. When transferring a Fermi gas produced in an optical dipole trap (ODT) into the lattice, the ODT and lattice potentials are jointly varied so that the ratio between the atom temperature and the lattice depth changes, which determines the final occupation ratio of the different lattice bands.

II. EXPERIMENTAL SETUP AND METHODS

The experimental setup is shown in Fig. 1. A single-frequency linearly polarized laser at $\lambda = 1064$ nm with a typical linewidth of 1 kHz (Coherent Prometheus 100NE) is used to form a 1D optical lattice. After passing through an acousto-optic modulator (CETC SGT80-1064-1TA), the laser is coupled into a single-mode polarization-maintaining fiber with a coreless end cap to ensure that the induced optical lattice has a good Gaussian distribution under a higher laser power. To keep the power of the two beams for the lattice stable, two pairs of the half waveplate and polarizing beam splitter are placed behind the collimator. Then the beam is split into two beams of the same power and polarization (z axis). The two beams travel through roughly the same optical path and are focused by the lens into the center of the experimental chamber. Thus the potential for trapping atoms in the center of the chamber is a combination of an optical lattice in the x axis (lattice axial direction) and Gaussian-shape confinement in the yz plane (lattice radial direction). At the bottom of each lattice site, the potential is nearly harmonic. In our experiment, the angle between the two crossed beams is $2\theta = 20°$. The power of each beam is 0.53 W and the Gaussian radius of the beam is about 123 μm in the center of the chamber. The lattice constant $d = \lambda/(2\sin\theta) = 3.06$ μm. The maximum trap depth value is $127.3E_R$, where $E_R = (2\pi\hbar\sin\theta)^2/2m\lambda^2$ is the recoil energy, with $\hbar$ the Planck constant and m the mass of the 6Li atom. Atoms are typically trapped at 1/3 of the diameter of a Gaussian beam, as shown in Fig. 1.

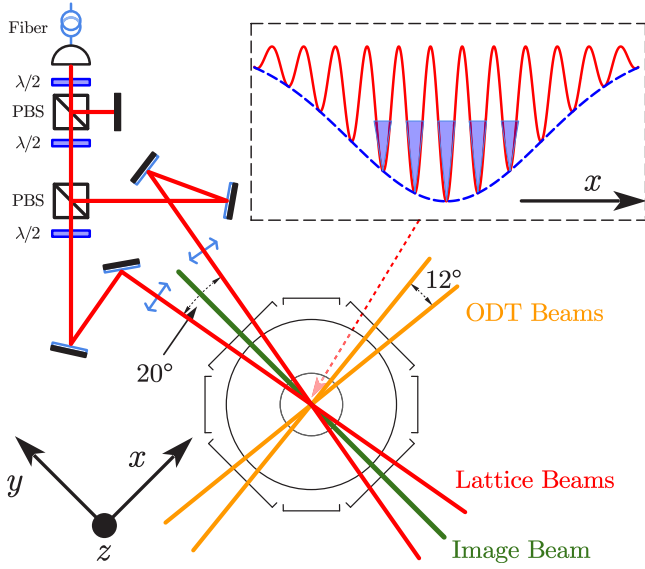*lijiam29@mail.sysu.edu.cn
†luole5@mail.sysu.edu.cn

FIG. 1. Schematic diagram of the experimental setup for a 1D optical lattice, the ODT, and the absorption image beam. The lattice potential is shown in the inset. Here PBS is the polarizing beam splitter and $\lambda/2$ is the half waveplate.

In our case, the axial length forming the lattice is about 83 µm, forming about 27 lattice sites. The average depth of the lattice is $U_0 = 118.6E_R = 5.4\hbar\omega_x = 5k_B$ µK, where k_B is the Boltzmann constant. In the following, we ignore the difference between the lattice sites and treat each lattice site as the same, using the average lattice depth. Each lattice site is strongly anisotropic and the ratio of trap frequencies of the central site is $\omega_x:\omega_y:\omega_z \approx 514:1:5.76$. When the trap depth value is $60E_R$, the tunneling time is 5 s [1], which is much longer than the typical 2D experimental time of 100 ms. Therefore, when the trap depth is more than $60E_R$, tunneling between the different lattice sites is negligible and the Fermi gas remains kinematically two dimensional.

We produce the ultracold Fermi gases in the ODT [28,29] and transfer gases to a 1D optical lattice to produce quasi-2D degenerate Fermi gases. The crossed-beam ODT with a crossed angle of $12°$ is made by a 100 W fiber laser at 1064 nm (IPG Photonics YLR-100-LP). The Gaussian radius of the beams at the center of the chamber is 37 µm. The maximum ODT depth is $5.6k_B$ mK. As shown in Fig. 2, a typical experimental procedure is described in the following steps. First, about 2×10^8 atoms at a temperature of 300 µK are trapped in a magneto-optical trap (MOT). Second, we transfer the atoms from the MOT to the ODT for evaporative cooling, typically lowering the ODT depth to several µK. In our experiment, we use the two lowest-energy hyperfine ground states of ^{6}Li, $|2\,^2S_{1/2}, F = 1/2, m_F = 1/2\rangle$ and $|2\,^2S_{1/2}, F = 1/2, m_F = -1/2\rangle$, usually labeled $|1\rangle$ and $|2\rangle$, respectively. A radio-frequency pulse is then applied to produce a 50:50 mixture of atoms in $|1\rangle$ and $|2\rangle$. At this point, there are about 5×10^5 atoms per spin state in the ODT. Third, starting from the ODT depth dropping to several µK, we ramp up the lattice depth from 1 µK to 4.4 µK with an exponential ramp of 160 ms, while the ODT is kept for 100 ms before turning off. Afterward, the lattice depth is kept stationary for 90 ms. Then the lattice depth is exponentially decreased to the desired
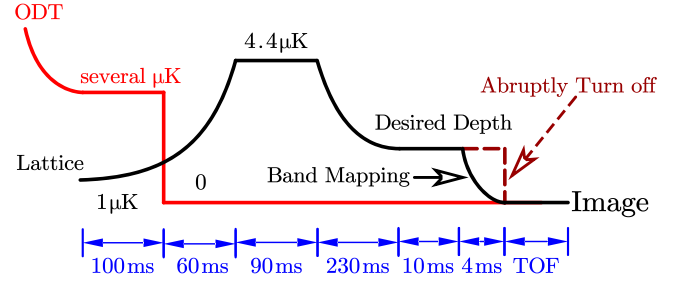

FIG. 2. Experimental sequence for the production of 2D-3D crossover Fermi gases. We keep the lattice depth for 10 ms and wait for thermal equilibrium when the lattice depth reaches the desired depth. After that, we choose to abruptly turn off the lattice or implement band mapping; then the absorption image is taken after the atom cloud expands in a magnetic curvature.

depth at 230 ms for further evaporative cooling. Eventually, we have about 1.5×10^5 atoms per spin state in the lattice.

In ultracold Fermi gases, we can realize two different types of the 2D-3D dimensional crossovers. One is band-occupation dimensional crossover and the other is interparticle-scattering dimensional crossover. Band-occupation type refers to the atoms occupying different energy bands in the lattice. A noninteracting Fermi gas is kinematically two dimensional when the effective global chemical potential of the gas $\mu < 3/2\hbar\omega_x$, where the atoms occupy only the lowest-energy band. Here $\hbar\omega_x$ is the energy-level gap from the ground state to the first excited state in the tight-binding direction. At zero temperature, the maximum number of atoms allowed in each lattice site satisfying the 2D condition is $N_{2D} = \eta(\eta + 1)/2$ [2], where $\eta = \omega_x/\sqrt{\omega_y\omega_z}$. When $\mu > 3/2\hbar\omega_x$, atoms occupy multiple energy bands and the Fermi gases are in the so-called the kinematic 2D-3D crossover. On the other hand, interparticle-scattering dimensional crossover means that the characteristic length of the lattice potential in the tight-binding direction is smaller than the scattering length between particles, where not only the kinematics but also the microscopic scattering properties of the atoms will be strongly modified by the lattice potential. In this paper we are focusing on the band-occupation dimensional crossover using noninteracting Fermi gas.

In our experiment, when we load the lowest-temperature Fermi gas into the lattice, the typical value of the atoms in each lattice site is about 5.5×10^3, which is much less than the $N_{2D} = 2.3 \times 10^4$ calculated using our trap parameters. So loading the lowest-temperature gas into the 1D lattice strictly produces a 2D Fermi gas. To approach the 2D-3D crossover, we could increase the occupation number of the atoms in the higher bands by increasing the ODT depth so the gas is hotter when loading into the lattice and the atoms have enough energy to occupy the higher bands, where the gas is located in the 2D-3D crossover. To tune the gas closer to the 2D side, we could further lower the lattice depth after the loading and the atoms in the higher band continue to evaporate so that the occupation ratio of the ground lattice band increases.

The band occupation information is obtained by taking the absorption images. Currently we cannot directly take individual images of each lattice site because of the resolution of the imaging system. So we take the images with two methods.
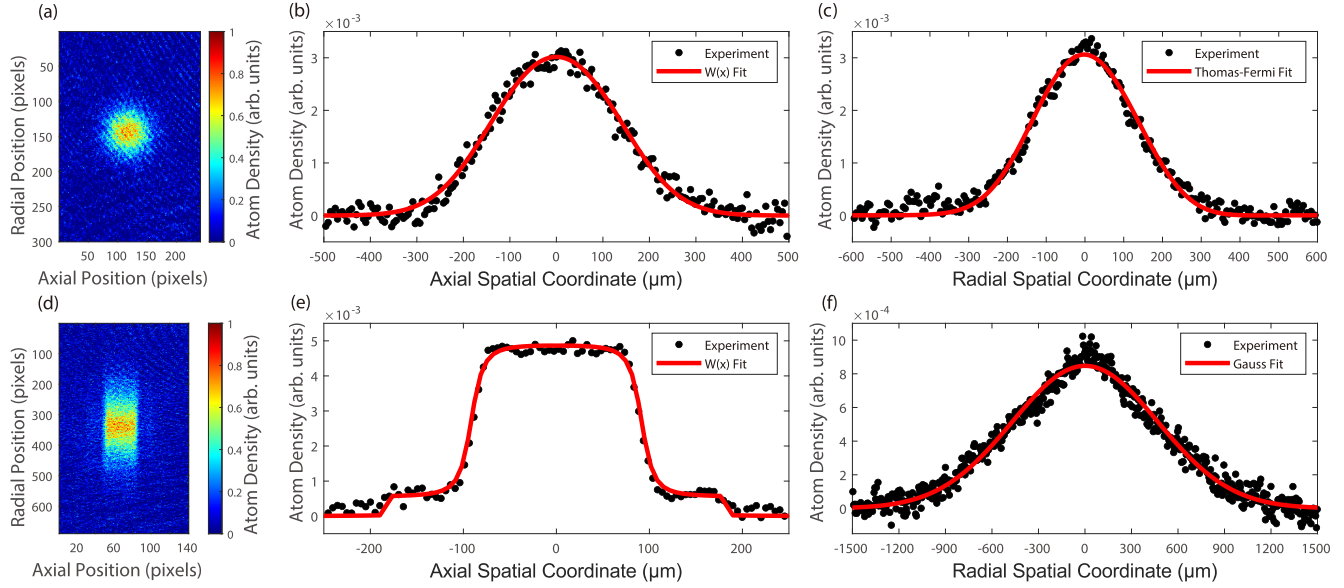
FIG. 3. Comparison of the (a)–(c) abrupt turnoff and (d)–(f) band mapping images, with the (a) and (d) column density, (b) and (e) axial, and (c) and (f) radial spatial density distribution (normalized) of an atom cloud occupying both the ground and first excited states of the lattice. Note that for the band mapping picture (e), a small population of the excited state is observed. The two clouds are captured by the ballistic expansion of atoms for 5 ms in (a) and the band mapping of atoms for 2.8 ms in (b). The other parameters for these images are described in the text.

One is to abruptly turn off the lattice, let the atom cloud expand for the time of flight (TOF), and then take the images. The other one is band mapping [30–36], in which the chemical potential and the ratio of the atoms occupying the different lattice bands can be obtained. The band mapping is achieved by gradually ramping down the lattice potential adiabatically over a suitable timescale. This timescale needs to be faster than the tunneling time of the lowest-energy band of the lattice so that the occupations of the different quasimomentum states remain constant during the lowering process. In addition, this timescale also needs to be slow enough so that different quasimomentum states can be adiabatically transformed into the corresponding momentum states. By doing this, the Bloch waves in the lattice will adiabatically transform into the plane waves. Correspondingly, the quasimomentum distribution of atoms in the lattice is transformed into the momentum distribution of the atoms when the lattice is off. Following a ballistic expansion after the band mapping, the momentum distribution is then transformed into the spatial density distribution of the atoms.

We first take the image by abruptly turning off the lattice, as shown in Fig. 3(a). The TOF after abrupt turnoff is 5 ms, which is a trade-off to obtain more image data points and maintain a high signal-to-noise ratio. The lattice depth before turnoff is $105E_R$ and the bias magnetic field during expansion is 300 G. The axial and radial distributions are shown in Figs. 3(b) and 3(c), respectively. The temperature of the gas is obtained from the radial distribution by fitting with the 2D Thomas-Fermi distribution. The radial spatial density distribution can be described by [1,37]

$$n(z) = -\frac{2N_a}{\sqrt{\pi}\sigma_z}\left(\frac{T}{T_F}\right)^{3/2}\mathrm{Li}_{3/2}\left[-\exp\left(\frac{\mu/E_F - z^2/\sigma_z^2}{T/T_F}\right)\right],$$

(1)

where $\sigma_z = \sqrt{2E_F/m\omega_z^2}$ is the Fermi radius, $E_F = \hbar\bar{\omega}\sqrt{2N_a}$ is the Fermi energy, $\bar{\omega} = \sqrt{\omega_y\omega_z}$, N_a is the number of atoms per spin state in a lattice site, $T_F = E_F/k_B$ is the Fermi temperature, and $\mathrm{Li}(x)$ is the polylogarithm. The T/T_F fitted by the 2D Thomas-Fermi distribution in Fig. 3(c) is 0.66 ± 0.06, which indicates that the temperature is 359 ± 31 nK.

Second, we implement the band mapping by ramping down the lattice potential to $0.01U_0 = 1.186E_R$ with an exponential ramp of 2.8 ms, as shown in Fig. 3(d). When the lattice depth is $1.186E_R$, the absolute depth of the lattice is no longer enough to trap the atoms and the atoms begin to expand. After that, the lattice is turned off and the atoms expand freely before taking the images. The TOF after band mapping is 12.8 ms. The axial and radial distributions are shown in Figs. 3(e) and 3(f), respectively. As shown in Fig. 3(e), the atoms are in a step distribution in the lattice axial direction. The radial distribution is about a Gaussian distribution, as shown in Fig. 3(f).

Based on the images in Fig. 3, we calculate the momentum distribution at the initial moment when the atom is just released from the optical lattice by the Wigner function $W(x, p, t)$ method [35,38]. When the atoms are released, the momentum distribution $W(p)$ of the atoms is converted to a spatial distribution $W(x)$. When the gas expands, the magnetic field does not shut down, so the expansion is affected by the magnetic-field curvature, which acts as a harmonic trap. For release into a harmonic potential, the Wigner function $W(x, p, t)$ rigorously obeys the equation of motion for a classical phase-space distribution. Thus $W(x, t)$ is determined by both the momentum distribution and the position distribution at the initial moment $W(x, p, t = 0)$. For imaging after a time of flight t, the final position distribution determines the momentum distribution when the final position distribution
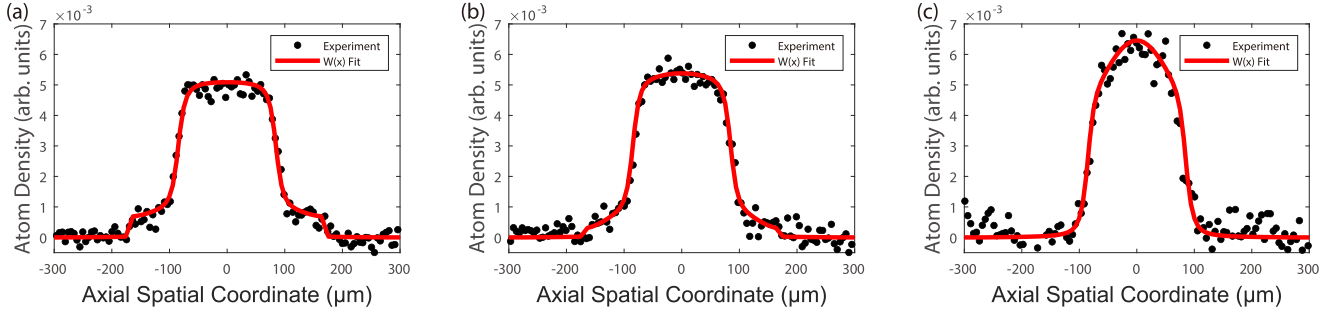
FIG. 4. Atom spatial density distribution in the lattice axial direction when the lattice depth changes. (a) The lattice depth is $14.1E_R$, similar to Fig. 3; the fitting gives $\mu = 13.7 \pm 0.2E_R > 3/2\hbar\omega_x = 11.3E_R$, $T/T_F = 0.70 \pm 0.10$, and $T = 99 \pm 14$ nK; and about 87% of the atoms are in the lowest band. (b) The lattice depth is $9.6E_R$, $\mu = 10.0 \pm 0.1E_R \approx 3/2\hbar\omega_x = 9.3E_R$, $T/T_F = 0.72 \pm 0.03$, $T = 75 \pm 3$ nK, and about 91% of the atoms are in the lowest band. (c) The lattice depth is $4.5E_R$, $\mu = 4.5 \pm 0.3E_R < 3/2\hbar\omega_x = 6.3E_R$, $T/T_F = 0.84 \pm 0.44$, $T = 50 \pm 27$ nK, and all the atoms are in the lowest band. The numbers of atoms are (a) 1.2×10^5, (b) 1.0×10^5, and (c) 7×10^4. As the lattice depth decreases, the atoms in the higher bands escape from the lattice.

is broad compared to the initial position distribution. For $\omega_{\text{mag}} t = \pi/2$, a quarter period, the final position distribution rigorously corresponds to the initial momentum distribution with the relation $p = m\omega_{\text{mag}} x / \sin(\omega_{\text{mag}} t)$, where ω_{mag} is the frequency of the magnetic trapping potential in the lattice axial direction and is independent of the initial position distribution. In our experiments, we control the expansion time t close to $T/4$ to neglect the effect of the initial position distribution.

The Wigner function related to the momentum distribution of atoms in the lattices is given by

$$W(p) = \frac{1}{\hbar} \sum_{\alpha,q} P^\mu_\alpha(q) \sum_G |C^\alpha_{q+G}|^2 \delta\left(\frac{p}{\hbar} - q - G\right), \quad (2)$$

where δ is the Dirac delta function and C^α_{q+G} is a coefficient determined by the Bloch wave function in a 1D optical lattice with

$$\psi^\alpha_q(x) = \frac{1}{\sqrt{Nd}} \sum_G C^\alpha_{q+G} \exp[i(q+G)x]. \quad (3)$$

We obtain the value of C^α_{q+G} by solving the time-independent Schrodinger equation in a 1D lattice [35], where N is the total number of lattice sites, d is the lattice constant, α is the band index, $q = 2n\pi/Nd$ is the quasimomentum in the lattice $-\pi/d \leqslant q \leqslant \pi/d$, $G = 2n\pi/d$ is the reciprocal lattice vector, and n is an integer.

Here $P^\mu_\alpha(q)$ is the probability that the atom is in the Bloch state with quasimomentum q and band index α when the chemical potential is μ. In our experiment, we treat the gas with zero temperature, so the probability can be described by

$$P^\mu_\alpha(q) = \frac{[\mu - E_\alpha(q)]^2}{\sum_{\alpha,q}[\mu - E_\alpha(q)]^2} \Theta(\mu - E_\alpha(q)), \quad (4)$$

where $E_\alpha(q)$ is the energy of the atom in the Bloch state with quasimomentum q and band index α and Θ is the Heaviside step function. In Fig. 3(b), $P^\mu_\alpha(q)$ and C^α_{q+G} of Eq. (2) both correspond to the lattice depth before it is abruptly turned off. In Fig. 3(e), $P^\mu_\alpha(q)$ still corresponds to the lattice depth before the tarp is lowered, but C^α_{q+G} corresponds to the lattice depth after band mapping.

Fitting Fig. 3(b) gives $\mu = 44.0 \pm 1.0E_R$ and about 84% of the atoms are in the lowest band. Fitting Fig. 3(e) gives $\mu = 39.1 \pm 0.3E_R > 3/2\hbar\omega_x = 30.7E_R$ and about 90% of the atoms are in the lowest band. Notice that the TOFs of the two images are different, which may result in the different effects of the initial spatial distribution on the momentum distribution. In Fig. 3(e) the TOF is close to $T/4$, corresponding to $\omega_{\text{mag}}/2\pi = 18.8 \pm 0.3$ Hz, so the effect of the initial spatial distribution is minimized [35,39].

III. RESULTS AND DISCUSSIONS

To tune the occupation of the ratio in the lowest lattice band, we adopts two experiments. The first one is to change the depth of the lattice when we abruptly turn off the ODT. We fix the ODT with a depth of $80E_R$ around 2.6% of the full ODT depth and load the atom into a lattice of a maximum depth of $25E_R$, where the atoms are relatively cold and most of them occupy the two lowest lattice bands. As shown in Fig. 4, when the lattice is lowered from Fig. 4(a) to Fig. 4(c), the atoms in the higher bands will evaporate, leading to an increase in the percentage of atoms occupying the lowest band.

In Fig. 5(a) we decrease the lattice depth and plot the dependence of the percentage of atoms in the lowest band and T/T_F of the atoms loaded into the lattice. When the lattice depth is above $8E_R$, the percentage of atoms in the lowest band does not vary significantly with the decrease of the trap depth, because the lattice depth is larger than the energy of the p band and the weakly interacting atoms do not have a large evaporative effect. This observation is also supported by the almost unchange T/T_F in this regime. Below $8E_R$, the percentage of atoms in the lowest band increases significantly with the decrease of the lattice depth, where it changes from around 85% to near the unity. The reason is that when the lattice depth approaches $7.5E_R$ it no longer supports the first excited band and so most of the atoms in the excited bands evaporate and in the end almost all the atoms are in the lowest band.

The second experiment is to tune the occupation of the energy band by varying the gas temperature in the ODT. The gas temperature is varied by changing the ODT depth when loading the lattice, where the higher lattice depth gives
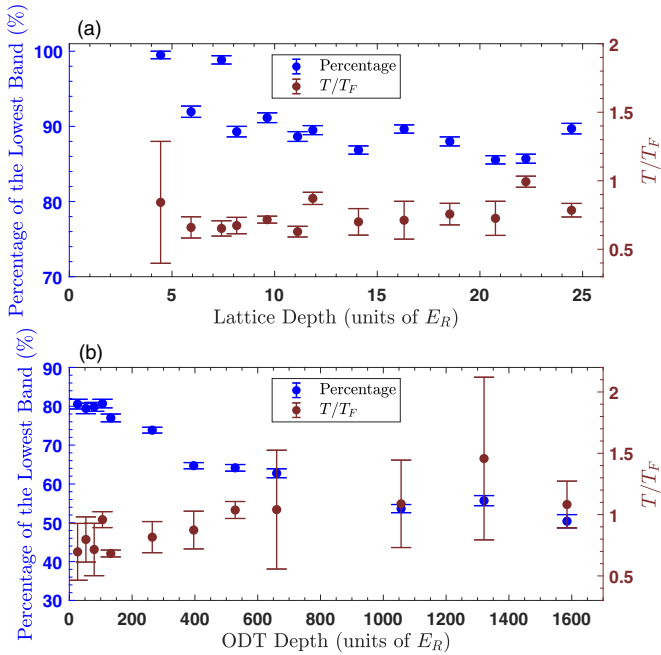
FIG. 5. Percentage of atoms occupying the lowest band and T/T_F of Fermi gases versus (a) the lattice depth before the band mapping and (b) the ODT depth when loading the lattice. Note that the percentage data in (b) are derived from the fitting of the axial distribution of the abrupt turnoff. All the error bars of data are the one standard deviation of the image fitting. The TOF is slightly less than $T/4$, so the fitting has a certain systematic error.
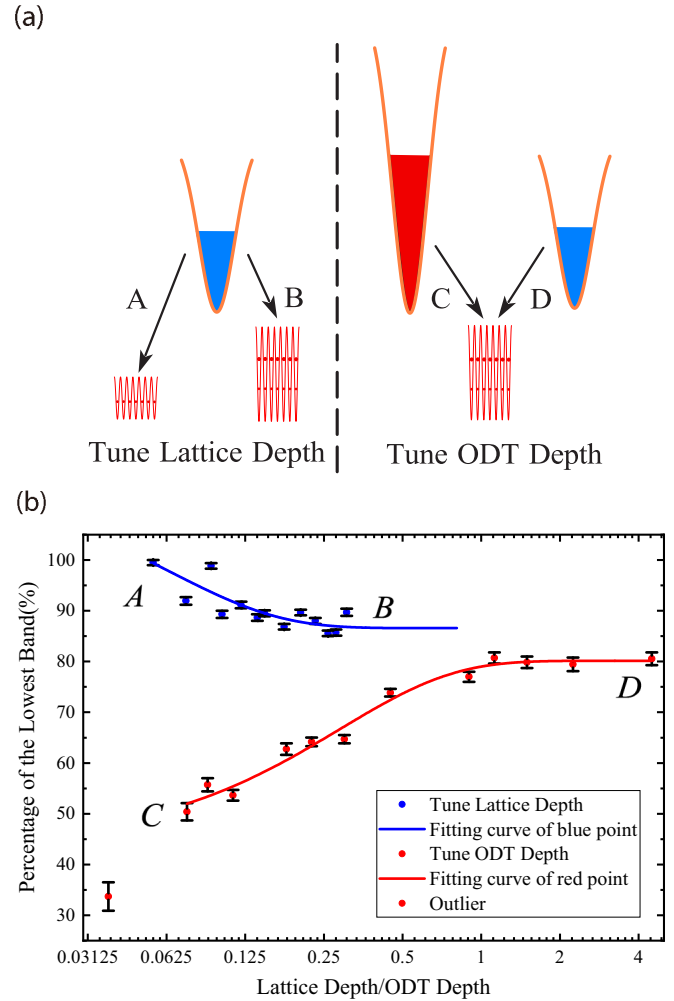

FIG. 6. Continuous tuning of the occupation ratio of the lowest band: (a) the experimental scheme and (b) the result. Note that the lowest red point in (b) is an outlier, which we cannot fit with a smooth curve. For that point, we load a very hot gas into a very shallow trap and the smooth evolution of the occupation ratio breaks. By varying the lattice depth, we could prepare a Fermi gas with the percentage of the atoms in the lowest band from unity to 80%. By varying the ODT depth, we could change the percentage from 80% to 50%.

a higher gas temperature. For example, we load a lattice of $119E_R$ with an ODT around $26E_R$, where we increase the ODT depth to change the percentage of atoms occupying the lowest band. As shown in Fig. 5(b), when the ODT depth increases, the gas is hotter and more atoms occupy higher-energy bands, resulting in a significant decrease of the percentage of atoms in the lowest band. Since the T/T_F of the gas in the ODT is higher, we observe that the T/T_F in the lattice is also higher.

The percentage of atoms occupying the lowest-energy band can be well controlled by jointly tuning the lattice depth and the ODT depth as shown in Fig. 6(a). We find that the percentage of atoms occupying the lowest-energy band strongly depends on the ratio of the lattice depth and the ODT depth. As shown in Fig. 6(b), there are two scenarios to adjust the percentage. First, for the loading with the shallow ODT, when we lower the lattice depth, the first excited energy band gradually approaches the edge of the lattice and atoms in the excited band will evaporate quickly so that the percentage of atoms occupying the lowest-energy band approaches unity. Second, for the deep trap loading, we increase the ODT depth and the lattice depth remains relatively high. As the ODT depth increases, more and more energetic atoms are transferred to the lattice and occupy the excited energy band, leading to a decrease in the percentage of atoms in the lowest-energy band. In experiments, we could choose to jointly tune the lattice depth and the ODT depth so that the percentage of atoms occupying the lowest-energy band, the temperature of the Fermi gas, and the number of atoms are all well controlled.

IV. SUMMARY

In summary, we have produced a degenerate Fermi gas in the 2D-3D crossover by transforming a Fermi gas from the ODT into a 1D optical lattice. We developed the method to quantitatively control the percentage of atoms in the lowest lattice band by jointly tuning the lattice depth and the ODT depth. The capability enables us to tune the Fermi gases in the crossover from two dimensions to three dimensions for further research on a many-body quantum system in the dimensionality crossover.

ACKNOWLEDGMENTS

[1] K. Martiyanov, V. Makhalov, and A. Turlapov, Observation of a Two-Dimensional Fermi Gas of Atoms, Phys. Rev. Lett. **105**, 030404 (2010).

[2] P. Dyke, E. D. Kuhnle, S. Whitlock, H. Hu, M. Mark, S. Hoinka, M. Lingham, P. Hannaford, and C. J. Vale, Crossover from 2D to 3D in a Weakly Interacting Fermi Gas, Phys. Rev. Lett. **106**, 105304 (2011).

[3] K. Günter, T. Stöferle, H. Moritz, M. Köhl, and T. Esslinger, *p*-Wave Interactions in Low-Dimensional Fermionic Gases, Phys. Rev. Lett. **95**, 230401 (2005).

[4] Y. Zhang, W. Ong, I. Arakelyan, and J. E. Thomas, Polaron-to-Polaron Transitions in the Radio-Frequency Spectrum of a Quasi-Two- Dimensional Fermi Gas, Phys. Rev. Lett. **108**, 235302 (2012).

[5] M. Koschorreck, D. Pertot, E. Vogt, B. Fröhlich, M. Feld, and M. Köhl, Attractive and repulsive Fermi polarons in two dimensions, Nature (London) **485**, 619 (2012).

[6] V. Makhalov, K. Martiyanov, and A. Turlapov, Ground-State Pressure of Quasi-2D Fermi and Bose Gases, Phys. Rev. Lett. **112**, 045301 (2014).

[7] K. Martiyanov, T. Barmashova, V. Makhalov, and A. Turlapov, Pressure profiles of nonuniform two-dimensional atomic Fermi gases, Phys. Rev. A **93**, 063622 (2016).

[8] I. Boettcher, L. Bayha, D. Kedar, P. A. Murthy, M. Neidig, M. G. Ries, A. N. Wenz, G. Zürn, S. Jochim, and T. Enss, Equation of State of Ultracold Fermions in the 2D BEC-BCS Crossover Region, Phys. Rev. Lett. **116**, 045303 (2016).

[9] K. Fenech, P. Dyke, T. Peppler, M. G. Lingham, S. Hoinka, H. Hu, and C. J. Vale, Thermodynamics of an Attractive 2D Fermi Gas, Phys. Rev. Lett. **116**, 045302 (2016).

[10] M. Feld, B. Fröhlich, E. Vogt, M. Koschorreck, and M. Köhl, Observation of a pairing pseudogap in a two-dimensional Fermi gas, Nature (London) **480**, 75 (2011).

[11] B. Fröhlich, M. Feld, E. Vogt, M. Koschorreck, W. Zwerger, and M. Köhl, Radio-Frequency Spectroscopy of a Strongly Interacting Two-Dimensional Fermi Gas, Phys. Rev. Lett. **106**, 105301 (2011).

[12] A. T. Sommer, L. W. Cheuk, M. J. H. Ku, W. S. Bakr, and M. W. Zwierlein, Evolution of Fermion Pairing from Three to Two Dimensions, Phys. Rev. Lett. **108**, 045302 (2012).

[13] S. K. Baur, B. Fröhlich, M. Feld, E. Vogt, D. Pertot, M. Koschorreck, and M. Köhl, Radio-frequency spectra of Feshbach molecules in quasi-two-dimensional geometries, Phys. Rev. A **85**, 061604(R) (2012).

[14] W. Ong, C. Cheng, I. Arakelyan, and J. E. Thomas, Spin-Imbalanced Quasi-Two-Dimensional Fermi Gases, Phys. Rev. Lett. **114**, 110403 (2015).

[15] M. G. Ries, A. N. Wenz, G. Zürn, L. Bayha, I. Boettcher, D. Kedar, P. A. Murthy, M. Neidig, T. Lompe, and S. Jochim, Observation of Pair Condensation in the Quasi-2D BEC-BCS Crossover, Phys. Rev. Lett. **114**, 230401 (2015).

[16] P. A. Murthy, I. Boettcher, L. Bayha, M. Holzmann, D. Kedar, M. Neidig, M. G. Ries, A. N. Wenz, G. Zürn, and S. Jochim, Observation of the Berezinskii-Kosterlitz-Thouless Phase Transition in an Ultracold Fermi Gas, Phys. Rev. Lett. **115**, 010401 (2015).

[17] D. Mitra, P. T. Brown, P. Schauß, S. S. Kondov, and W. S. Bakr, Phase Separation and Pair Condensation in a Spin-Imbalanced 2D Fermi Gas, Phys. Rev. Lett. **117**, 093601 (2016).

[18] P. A. Murthy, M. Neidig, R. Klemt, L. Bayha, I. Boettcher, T. Enss, M. Holten, G. Zürn, P. M. Preiss, and S. Jochim, High-temperature pairing in a strongly interacting two-dimensional Fermi gas, Science **359**, 452 (2018).

[19] M. Koschorreck, D. Pertot, E. Vogt, and M. Köhl, Universal spin dynamics in two-dimensional Fermi gases, Nat. Phys. **9**, 405 (2013).

[20] M. Bohlen, L. Sobirey, N. Luick, H. Biss, T. Enss, T. Lompe, and H. Moritz, Sound Propagation and Quantum-Limited Damping in a Two-Dimensional Fermi Gas, Phys. Rev. Lett. **124**, 240403 (2020).

[21] L. Sobirey, N. Luick, M. Bohlen, H. Biss, H. Moritz, and T. Lompe, Observation of superfluidity in a strongly correlated two-dimensional Fermi gas, Science **372**, 844 (2021).

[22] E. Vogt, M. Feld, B. Fröhlich, D. Pertot, M. Koschorreck, and M. Köhl, Scale Invariance and Viscosity of a Two-Dimensional Fermi Gas, Phys. Rev. Lett. **108**, 070404 (2012).

[23] M. Holten, L. Bayha, A. C. Klein, P. A. Murthy, P. M. Preiss, and S. Jochim, Anomalous Breaking of Scale Invariance in a Two-Dimensional Fermi Gas, Phys. Rev. Lett. **121**, 120401 (2018).

[24] T. Peppler, P. Dyke, M. Zamorano, I. Herrera, S. Hoinka, and C. J. Vale, Quantum Anomaly and 2D-3D Crossover in Strongly Interacting Fermi Gases, Phys. Rev. Lett. **121**, 120402 (2018).

[25] P. A. Murthy, N. Defenu, L. Bayha, M. Holten, P. M. Preiss, T. Enss, and S. Jochim, Quantum scale anomaly and spatial coherence in a 2D Fermi superfluid, Science **365**, 268 (2019).

[26] N. Luick, L. Sobirey, M. Bohlen, V. P. Singh, L. Mathey, T. Lompe, and H. Moritz, An ideal Josephson junction in an ultracold two-dimensional Fermi gas, Science **369**, 89 (2020).

[27] C. Cheng, J. Kangara, I. Arakelyan, and J. E. Thomas, Fermi gases in the two-dimensional to quasi-two-dimensional crossover, Phys. Rev. A **94**, 031606(R) (2016).

[28] J. Li, J. Liu, W. Xu, L. de Melo, and L. Luo, Parametric cooling of a degenerate Fermi gas in an optical trap, Phys. Rev. A **93**, 041401(R) (2016).

[29] J. Li, J. Liu, L. Luo, and B. Gao, Three-Body Recombination near a Narrow Feshbach Resonance in ⁶Li, Phys. Rev. Lett. **120**, 193402 (2018).

[30] S. S. Natu, D. C. McKay, B. DeMarco, and E. J. Mueller, Evolution of condensate fraction during rapid lattice ramps, Phys. Rev. A **85**, 061601(R) (2012).

[31] M. Greiner, I. Bloch, O. Mandel, T. W. Hänsch, and T. Esslinger, Exploring Phase Coherence in a 2D Lattice of Bose-Einstein Condensates, Phys. Rev. Lett. **87**, 160405 (2001).

[32] M. Köhl, H. Moritz, T. Stöferle, K. Günter, and T. Esslinger, Fermionic Atoms in a Three Dimensional Optical Lattice: Observing Fermi Surfaces, Dynamics, and Interactions, Phys. Rev. Lett. **94**, 080403 (2005).

[33] M. H. G. de Miranda, Control of dipolar collisions in the quantum regime, Ph.D. thesis, University of Colorado, 2010.

[34] B. Fröhlich, A strongly interacting two-dimensional Fermi gas, Ph.D. thesis, University of Cambridge, 2011.

[35] C. Cheng, Ultracold Fermi gases in a bichromatic optical superlattice, Ph.D. thesis, Duke University, 2016.

[36] M. Waseem, Collisional properties of Fermi gases with *p*-wave interactions, Ph.D. thesis, University of Electro-Communications, Tokyo, 2018.

[37] J. M. Kinast, Thermodynamics and superfluidity of a strongly interacting Fermi gas, Ph.D. thesis, Duke University, 2006.

[38] W. Case, Wigner functions and Weyl transforms for pedestrians, Am. J. Phys. **76**, 937 (2008).

[39] P. A. Murthy, D. Kedar, T. Lompe, M. Neidig, M. G. Ries, A. N. Wenz, G. Zürn, and S. Jochim, Matter-wave Fourier optics with a strongly interacting two-dimensional Fermi gas, Phys. Rev. A **90**, 043611 (2014).